

On the Performance of Uplink ISAC Systems

Ch'ung-Chün Ouyang, Yuanwei Liu, and Hongwen Yang

Abstract—This letter analyzes the performance of uplink integrated sensing and communications (ISAC) systems where communication users (CUs) and radar targets (RTs) share the same frequency band. Novel expressions are derived to characterize the outage probability, ergodic communication rate, and sensing rate. Besides, the diversity order and high signal-to-noise ratio (SNR) slope are unveiled to gain more insights. It is found that when achieving the same communication rate, the ISAC system enjoys a higher sensing rate than the conventional frequency-division sensing and communications (FDSAC) system where CUs and RTs share isolated bands. All the results are validated by numerical simulations and are in excellent agreement.

Index Terms—Communication rate, integrated sensing and communications (ISAC), performance analysis, sensing rate.

I. INTRODUCTION

Integrated sensing and communications (ISAC) is believed to be a promising spectrum-sharing candidate for future wireless networks [1]. By integrating the wireless communications and radar sensing to share the same spectrum and infrastructure, ISAC is capable of improving the spectral efficiency, reducing the hardware cost, and limiting the electromagnetic pollution [1]. These advantages have attracted vibrant industrial and academic interest in the ISAC technique [2]–[4].

Recently, a considerable literature has grown up around the theme of ISAC. For a review, please see the recent overview papers [1]–[4] and references therein. Yet, it is worth noting that most studies in the field of ISAC have only focused on the waveform or beamforming design. In contrast to this, there has been little quantitative analysis of the basic performance of ISAC systems, while only a couple of papers appeared recently [5], [6]. For example, the communication-sensing performance tradeoffs in ISAC systems were discussed from an estimation-theoretical perspective by using the Cramér-Rao bound metric for radar sensing and minimum mean square error metric for communications [5]. On a parallel track, the communication-sensing rate region achieved in ISAC systems was characterized from an information-theoretical perspective [6]. In a nutshell, these works have laid a solid foundation for understanding the fundamental performance of ISAC systems. However, in these works, the influence of channel fading was not taken into account and no more in-depth system insights, such as the diversity order and high signal-to-noise ratio (SNR) slope, were unveiled.

To fill this knowledge gap, this letter investigates the fundamental performance of uplink ISAC systems by using the outage probability (OP) as well as the ergodic communication

C.-C. Ouyang and H. Yang are with the School of Information and Communication Engineering, Beijing University of Posts and Telecommunications, Beijing, 100876, China (e-mail: {DragonAim,yanghong}@bupt.edu.cn).

Y. Liu is with the School of Electronic Engineering and Computer Science, Queen Mary University of London, London, E1 4NS, U.K. (e-mail: yuanwei.liu@qmul.ac.uk).

rate (ECR) metrics for communications and maximal sensing rate metric for radar sensing. Particularly, we provide exact expressions for these metrics as well as their high-SNR approximations. Numerical results suggest that when achieving the same communication rate, the ISAC system yields a higher sensing rate than the frequency-division sensing and communications (FDSAC) system where isolated bands are used for communications and sensing, respectively.

II. SYSTEM MODEL

In an uplink ISAC system shown in Fig. 1(a), one radar-communications (RadCom) base station (BS) serves a set of $2K$ single-antenna communication users (CUs) while simultaneously sensing the radar targets (RTs) in the same frequency band. There are two types of CUs, namely near CUs and cell-edge CUs. Particularly, we assume the $2K$ CUs communicate with the BS under a signal alignment-based non-orthogonal multiple access (NOMA) protocol [7]. Moreover, the CUs are grouped into K groups and each group contains one near CU and one cell-edge CU, respectively [7]. Finally, the BS is assumed to be equipped with two spatially widely separated antenna arrays [8], [9], i.e., M transmit antennas and N receive antennas, whose structure is illustrated in Fig. 1(b).

The whole ISAC procedure can be divided into two stages. At first, the BS broadcasts the radar waveform $\mathbf{S} = [\mathbf{s}_1 \cdots \mathbf{s}_L] \in \mathbb{C}^{M \times L}$ ($L \geq M, L \geq N$) for sensing the nearby environment, where $\mathbf{s}_l \in \mathbb{C}^{M \times 1}$ denotes the waveform at time instant l . Besides, the radar waveform is subject to the power budget $\text{tr}(\mathbf{S}\mathbf{S}^H) \leq p_s$ with p_s denoting the sensing SNR. In the second stage, the BS receives the radar waveform reflected by RTs and the communication messages sent by CUs simultaneously. It is worth noting that the radar waveform reflected by CUs is assumed to be perfectly removed at the BS for the sake of brevity. Accordingly, the BS observes the following superposed signal matrix:

$$\mathbf{Y} = \sum_{k=1}^K (\mathbf{h}_k \mathbf{x}_k^H + \mathbf{h}_{k'} \mathbf{x}_{k'}^H) + \mathbf{G}^H \mathbf{S} + \mathbf{N}, \quad (1)$$

where $\mathbf{h}_i \in \mathbb{C}^{N \times 1}$ denotes the channel vector from CU i to the BS; $\mathbf{G} = [g_{i,j}] = [\mathbf{g}_1 \cdots \mathbf{g}_N] \in \mathbb{C}^{M \times N}$ denotes the channel matrix to be sensed with $g_{i,j}$ representing the target response from the i th transmit antenna to the j th receive antenna; $\mathbf{N} = [\mathbf{n}_1 \cdots \mathbf{n}_L] \in \mathbb{C}^{N \times L}$ denotes the additive white Gaussian noise (AWGN); $\mathbf{x}_i = [x_{i,1}, \dots, x_{i,L}]^H$ denotes the message sent by CU i with $\mathbb{E}\{|x_{i,j}|^2\} = p_c$ being the transmit SNR. We comment that in this letter only small-scale fading is considered, whereas large-scale path loss is omitted, i.e., each element of $\mathbf{h}_i \sim \mathcal{CN}(\mathbf{0}, \mathbf{I}_N)$ is independent and identically distributed (i.i.d.) complex Gaussian variables with zero mean and unit variance. Besides, we assume that

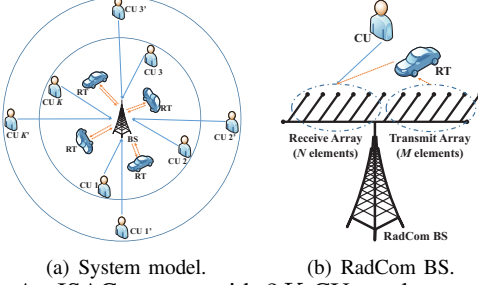


Fig. 1: An ISAC system with $2K$ CUs and several RTs.

the columns of \mathbf{N} and \mathbf{G} are i.i.d., with $\mathbf{n}_l \sim \mathcal{CN}(\mathbf{0}, \mathbf{I}_N)$ and $\mathbf{g}_n \sim \mathcal{CN}(\mathbf{0}, \mathbf{R}_T)$ ($\mathbf{R}_T \succ \mathbf{0}$). Besides, we assume the perfect channel state information (CSI) of CUs is available at the BS. On the contrary, since \mathbf{G} needs to be sensed, we only assume the covariance matrix \mathbf{R}_T is available at the BS [8], [9].

After the RadCom BS receives the superposed signal matrix \mathbf{Y} , it can leverage a successive interference cancellation (SIC)-based framework to decode the communication signals, \mathbf{x}_i , as well as sensing the channel matrix, \mathbf{G} [6]. Particularly, the BS first decodes \mathbf{x}_i by treating the radar waveform as interference. Then, \mathbf{x}_i can be subtracted from \mathbf{Y} and the rest part will be used for sensing \mathbf{G} . In the sequel, we will discuss the performance of communications and radar sensing, respectively.

III. PERFORMANCE OF COMMUNICATION SIGNALS

For simplicity, we only focus on the time instant i . In this case, equation (1) degenerates into

$$\mathbf{y}_i = \sum_{k=1}^K (\mathbf{h}_k x_{k,i} + \mathbf{h}_{k'} x_{k',i}) + \mathbf{G}^H \mathbf{s}_i + \mathbf{n}_i. \quad (2)$$

A. Inter-Group Interference Cancellation

We adopt the filtering matrix $\mathbf{W} = [\mathbf{w}_1, \dots, \mathbf{w}_K] \in \mathbb{C}^{N \times K}$ to decode the messages transmitted by each group in parallel. In this case, the data stream sent by the k th group is given by

$$y_{k,i} = \mathbf{w}_k^H (\mathbf{h}_k x_{k,i} + \mathbf{h}_{k'} x_{k',i}) + \sum_{j \neq k} \mathbf{w}_k^H (\mathbf{h}_j x_{j,i} + \mathbf{h}_{j'} x_{j',i}) + \mathbf{w}_k^H \mathbf{G}^H \mathbf{s}_i + n_{k,i}, \quad (3)$$

where $n_{k,i} \triangleq \mathbf{w}_k^H \mathbf{n}_i$. To avoid the inter-group interference (IGI), we assume $N \geq 2K$ and resort to the zero-forcing (ZF) combiner [7]. In this case, we have $\mathbf{w}_k = \frac{\mathbf{p}_k}{\|\mathbf{p}_k\|}$, where \mathbf{p}_k denotes the $(2k-1)$ th column of matrix $\mathbf{P}_k = \mathbf{H}_k (\mathbf{H}_k^H \mathbf{H}_k)^{-1}$ with \mathbf{H}_k being the sub-matrix of $\mathbf{H} = [\mathbf{h}_1 \mathbf{h}_1' \cdots \mathbf{h}_K \mathbf{h}_K']$ after removing the $(2k)$ th column, $\mathbf{h}_{k'}$. By the property of $\mathbf{I}_{2K-1} = \mathbf{H}_k^H \mathbf{P}_k$, we can simplify $y_{k,i}$ as

$$y_{k,i} = \mathbf{w}_k^H (\mathbf{h}_k x_{k,i} + \mathbf{h}_{k'} x_{k',i}) + \mathbf{w}_k^H \mathbf{G}^H \mathbf{s}_i + n_{k,i}. \quad (4)$$

Afterwards, the BS can decode the message $(x_{k,i}, x_{k',i})$ by employing SIC [7]. Notably, for uplink NOMA, the sum rate of each user group is always the same, no matter which decoding order is used [7]. Thus, assume that $x_{k,i}$ is decoded at first. From a worst-case design perspective [10], the aggregate interference-plus-noise $\mathbf{w}_k^H \mathbf{h}_{k'} x_{k',i} + \mathbf{w}_k^H \mathbf{G}^H \mathbf{s}_i + n_{k,i}$ is treated as the Gaussian noise. Besides, it is worthy mentioning that the RadCom BS has no full CSI of \mathbf{G} . Consequently, within

the k th group, $x_{k,i}$ can be decoded with the following signal-to-interference-plus-noise ratio (SINR)

$$\gamma_{k,i} = \frac{p_c |\mathbf{w}_k^H \mathbf{h}_k|^2}{p_c |\mathbf{w}_k^H \mathbf{h}_{k'}|^2 + \mathbb{E} \left\{ |\mathbf{w}_k^H \mathbf{G}^H \mathbf{s}_i|^2 + |n_{k,i}|^2 \right\}}, \quad (5)$$

whereas $x_{k',i}$ can be decoded with the following SINR

$$\gamma_{k',i} = \frac{p_c |\mathbf{w}_k^H \mathbf{h}_{k'}|^2}{\mathbb{E} \left\{ |\mathbf{w}_k^H \mathbf{G}^H \mathbf{s}_i|^2 + |n_{k,i}|^2 \right\}}. \quad (6)$$

Taken together, the communication rate of CU k , CU k' , and the k th CU group can be written as $\mathcal{R}_{k,i} = \log_2 (1 + \gamma_{k,i})$, $\mathcal{R}_{k',i} = \log_2 (1 + \gamma_{k',i})$, and $\mathcal{R}_{g,k,i} = \mathcal{R}_{k,i} + \mathcal{R}_{k',i} = \log_2 (1 + \gamma_{g,k,i})$ with $\gamma_{g,k,i} = \frac{p_c |\mathbf{w}_k^H \mathbf{h}_k|^2 + p_c |\mathbf{w}_k^H \mathbf{h}_{k'}|^2}{\mathbb{E} \left\{ |\mathbf{w}_k^H \mathbf{G}^H \mathbf{s}_i|^2 + |n_{k,i}|^2 \right\}}$, respectively. In the sequel, we intend to discuss the outage probability and the ergodic rate achieved by communication signals.

B. Outage Probability

The OPs of CU k , CU k' , and the k th group are given by

$$P_{k,i} = \Pr (\gamma_{k,i} < \bar{\gamma}_{k,i}), \quad (7a)$$

$$P_{k',i} = 1 - \Pr (\gamma_{k,i} > \bar{\gamma}_{k,i}, \gamma_{k',i} > \bar{\gamma}_{k',i}), \quad (7b)$$

$$P_{g,k,i} = \Pr (\gamma_{g,k,i} < \bar{\gamma}_{g,k,i}), \quad (7c)$$

respectively, where $\bar{\gamma}_{k,i} = 2^{\bar{\mathcal{R}}_{k,i}} - 1$, $\bar{\gamma}_{k',i} = 2^{\bar{\mathcal{R}}_{k',i}} - 1$, and $\bar{\gamma}_{g,k,i} = 2^{\bar{\mathcal{R}}_{g,k,i}} - 1$ with $\bar{\mathcal{R}}_{k,i}$, $\bar{\mathcal{R}}_{k',i}$, and $\bar{\mathcal{R}}_{g,k,i}$ being the target rates of CU k , CU k' , and the k th group, respectively. The following theorem provides exact expressions for these probabilities as well as their high-SNR approximations.

Theorem 1. The OPs $P_{k,i}$, $P_{k',i}$, and $P_{g,k,i}$ are given by

$$P_{k,i} = 1 - e^{-\frac{\bar{\gamma}_{k,i}}{\rho}} \sum_{l=0}^{N_K} \sum_{n=0}^l \frac{(\bar{\gamma}_{k,i}/\rho)^{l-n} \bar{\gamma}_{k,i}^n}{(l-n)! n! (\bar{\gamma}_{k,i} + 1)^{n+1}}, \quad (8a)$$

$$P_{k',i} = 1 - \sum_{l=0}^{N_K} \sum_{n=0}^l \frac{\left(\frac{1}{\rho}\right)^{l-n} \Gamma \left(n+1, \frac{\bar{\gamma}_{k',i}(\bar{\gamma}_{k,i}+1)}{\rho} \right)}{\bar{\gamma}_{k,i}^{-l} e^{\frac{\bar{\gamma}_{k,i}}{\rho}} (l-n)! n! (\bar{\gamma}_{k,i} + 1)^{n+1}}, \quad (8b)$$

$$P_{g,k,i} = \frac{1}{(N_K + 1)!} \Upsilon (N_K + 2, \bar{\gamma}_{g,k,i}/\rho), \quad (8c)$$

respectively, where $N_K = N - 2K + 1$, $\rho = \frac{p_c}{\sigma^2}$, $\sigma^2 = 1 + |\mathbf{s}_i^H \mathbf{R}_T \mathbf{s}_i|$, $\Gamma(s, x) = \int_x^\infty t^{s-1} e^{-t} dt$ denotes the upper incomplete gamma function [11, eq. 8.350.2], and $\Upsilon(s, x) = \int_0^x t^{s-1} e^{-t} dt$ denotes the lower incomplete gamma function [11, eq. 8.350.1]. If the transmit SNR p_c approaches infinity, the OPs satisfy:

$$\lim_{p_c \rightarrow \infty} P_{k,i} = \lim_{p_c \rightarrow \infty} P_{k',i} = 1 - \sum_{l=0}^{N_K} \frac{\bar{\gamma}_{k,i}^l / l!}{(\bar{\gamma}_{k,i} + 1)^{l+1}}, \quad (9a)$$

$$\lim_{p_c \rightarrow \infty} P_{g,k,i} = \left(\frac{\bar{\gamma}_{g,k,i} \sigma^2}{p_c} \right)^{N-2K+3} \frac{1}{(N-2K+3)!}. \quad (9b)$$

Proof: Please refer to Appendix A for more details. ■

Remark 1. The OPs of CU k and CU k' converge to the same floor in the high-SNR regime due to the principle of uplink NOMA, indicating their diversity orders are both zero.

Remark 2. A diversity order of $N - 2K + 3$ is achievable for the sum rate in the k th CU group, which can be improved by increasing the number of receive antennas, N .

C. Ergodic Communication Rate

The ECRs of CU k , CU k' , and the k th group are given by $\bar{\mathcal{R}}_{k,i} = \mathbb{E}\{\mathcal{R}_{k,i}\}$, $\bar{\mathcal{R}}_{k',i} = \mathbb{E}\{\mathcal{R}_{k',i}\}$, and $\bar{\mathcal{R}}_{g,k,i} = \mathbb{E}\{\mathcal{R}_{g,k,i}\}$, respectively. Theorem 2 provides exact expressions for the ECRs as well as their high-SNR approximations.

Theorem 2. The ECRs $\bar{\mathcal{R}}_{k',i}$, $\bar{\mathcal{R}}_{g,k,i}$, and $\bar{\mathcal{R}}_{k,i}$ are given by

$$\bar{\mathcal{R}}_{k',i} = -e^{1/\rho} \text{Ei}(-1/\rho) \log_2 e, \quad (10a)$$

$$\begin{aligned} \bar{\mathcal{R}}_{g,k,i} = & \sum_{n=0}^{\bar{N}_K-1} \frac{\log_2 e}{(\bar{N}_K - 1 - n)!} \left(-\frac{1}{\rho}\right)^{\bar{N}_K-n} \left[-e^{\frac{1}{\rho}} \right. \\ & \times \text{Ei}\left(-\frac{1}{\rho}\right) + \sum_{l=1}^{\bar{N}_K-1-n} (l-1)! (-\rho)^l \left. \right], \quad (10b) \end{aligned}$$

$$\bar{\mathcal{R}}_{k,i} = \bar{\mathcal{R}}_{g,k,i} - \bar{\mathcal{R}}_{k',i}, \quad (10c)$$

respectively, where $\bar{N}_K = N - 2K + 3$ and $\text{Ei}(x) = -\int_{-x}^{\infty} e^{-t} t^{-1} dt$ denotes the exponential integral function [11, eq. (8.211.1)]. If the transmit SNR p_c approaches infinity, the ECRs can be approximated as follows:

$$\bar{\mathcal{R}}_{k,i} \approx (\psi(\bar{N}_K) - \psi(1)) \log_2 e, \quad (11a)$$

$$\bar{\mathcal{R}}_{k',i} \approx \log_2(\rho) - \mathbf{C} \log_2 e, \quad (11b)$$

$$\bar{\mathcal{R}}_{g,k,i} \approx \log_2(\rho) + (\psi(\bar{N}_K) - \psi(1) - \mathbf{C}) \log_2 e, \quad (11c)$$

respectively, where $\psi(x) = \frac{d}{dx} \ln \Gamma(x)$ is the Digamma function [11, eq. (6.461)], $\Gamma(x) = \int_0^{\infty} t^{x-1} e^{-t} dt$ is the gamma function [11, eq. (6.1.1)], and \mathbf{C} denotes the Euler constant.

Proof: Please refer to Appendix B for more details. ■

Remark 3. The high-SNR slopes of CU k , CU k' , and the k th CU group are given by 0, 1, 1, respectively, which are not affected by the number of RadCom BS antennas.

Corollary 1. At time instant i , the ergodic sum communication rate of the $2K$ CUs satisfies $\bar{\mathcal{R}}_i = \sum_{k=1}^K \bar{\mathcal{R}}_{g,k,i} \approx K(\log_2(\rho) + (\psi(\bar{N}_K) - \psi(1) - \mathbf{C}) \log_2 e)$ as $p_c \rightarrow \infty$.

Remark 4. A high-SNR slope of K is achievable for the uplink sum rate of the K CU groups, which is independent of the BS antenna number.

D. Communication Performance of FDSAC

In this part, we consider FDSAC as a baseline scenario, where the total bandwidth is partitioned into two sub-bands according to some α , one for radar only and the other for communications. Particularly, we assume α fraction of the total bandwidth is used for communications with $\alpha \in [0, 1]$. Under this circumstance, the ergodic sum rate of the K groups can be written as $\bar{\mathcal{R}}_{c,f}^{\alpha} = \mathbb{E}\{\mathcal{R}_{c,f}^{\alpha}\}$ with $\mathcal{R}_{c,f}^{\alpha} = \sum_{k=1}^K \alpha \log_2 \left(1 + \left(\left|\mathbf{w}_k^H \mathbf{h}_k\right|^2 + \left|\mathbf{w}_k^H \mathbf{h}_{k'}\right|^2\right) p_c / \alpha\right)$. It is worth noting that $\bar{\mathcal{R}}_{c,f}$ can be analyzed by following a similar approach as that in analyzing $\bar{\mathcal{R}}_i$.

IV. PERFORMANCE OF RADAR SENSING

After decoding all the information bits sent by the CUs, the BS can remove the communication signal from the received superposed signal matrix in (1), and then the rest part can be used for radar sensing [6], which is expressed as

$$\mathbf{Y}_s = \mathbf{G}^H \mathbf{S} + \mathbf{N}. \quad (12)$$

Since \mathbf{Y}_s and \mathbf{S} are both available, the RadCom BS can leverage them to sense the channel \mathbf{G} . The corresponding sensing rate can be evaluated by the sensing mutual information per unit time [4]. In this letter, we assume that each waveform symbol lasts 1 unit time. Accordingly, the sensing rate can be mathematically characterized as \mathcal{I}_L/L , where \mathcal{I}_L denotes the sensing mutual information over the duration of L symbols. By definition, we can obtain [8, eq. (9)]

$$\mathcal{I}_L = I(\mathbf{Y}_s; \mathbf{G}|\mathbf{S}) = N \log_2 \det \left(\mathbf{I} + \mathbf{S}^H \mathbf{R}_T \mathbf{S} \right) \triangleq N \mathcal{I}_T, \quad (13)$$

where $I(X; Y|Z)$ denotes the mutual information between X and Y conditioned on Z . Consequently, the maximal achievable sensing rate satisfies

$$\mathcal{R}_s = \frac{N}{L} \max_{\text{tr}(\mathbf{S}\mathbf{S}^H) \leq p_s} \log_2 \det \left(\mathbf{I}_L + \mathbf{S}^H \mathbf{R}_T \mathbf{S} \right). \quad (14)$$

The following theorem provides an exact expression for the maximal sensing rate as well as its high-SNR approximation.

Theorem 3. The maximal achievable sensing rate of the considered ISAC system can be written as

$$\mathcal{R}_s = \frac{N}{L} \sum_{m=1}^M \log_2 (1 + \lambda_m s_m^*), \quad (15)$$

where $\{\lambda_m\}_{m=1}^M$ denote the eigenvalues of \mathbf{R}_T and $s_m^* = \max\{0, 1/\nu - 1/\lambda_i\}$ with ν satisfying $\sum_{m=1}^M \max\{0, 1/\nu - 1/\lambda_i\} = p_s$. The maximal sensing rate \mathcal{R}_s is achieved when the eigendecomposition (ED) of $\mathbf{S}\mathbf{S}^H$ satisfies $\mathbf{S}\mathbf{S}^H = \mathbf{U}_T^H \Delta^* \mathbf{U}_T$, where $\mathbf{U}_T^H \text{diag}\{\lambda_1, \dots, \lambda_M\} \mathbf{U}_T$ denotes the ED of \mathbf{R}_T with $\lambda_1 \geq \dots \geq \lambda_M > 0$ and $\Delta^* = \text{diag}\{s_1^*, \dots, s_M^*\}$. If the transmit SNR p_s approaches infinity, the maximal achievable sensing rate satisfies

$$\mathcal{R}_s \approx \frac{NM}{L} \left(\log_2 p_s + \frac{1}{M} \sum_{m=1}^M \log_2 \left(\frac{\lambda_m}{M} \right) \right). \quad (16)$$

Proof: Please refer to Appendix C for more details. ■

Remark 5. A high-SNR slope of $\frac{NM}{L}$ is achievable for the maximal achievable sensing rate, which can be improved by increasing the number of BS antennas.

Corollary 2. When the optimal radar waveform matrix is adopted, the interference from the radar signals to the communication signals can be simplified as follows:

$$\mathbb{E} \left\{ \left| \mathbf{w}_k^H \mathbf{G}^H \mathbf{s}_i \right|^2 \right\} = \begin{cases} s_i^* \lambda_i & 1 \leq i \leq M \\ 0 & M < i \leq L \end{cases}. \quad (17)$$

Proof: Please refer to Appendix D for more details. ■

Remark 6. The results in Corollary 2 suggest that the optimal radar waveform will not influence the quality of service of communication signals at time instant i ($L \geq i > M$).

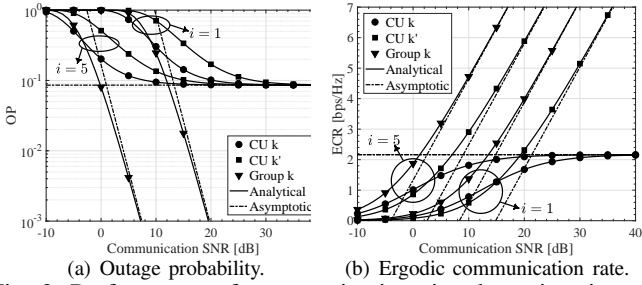


Fig. 2: Performance of communication signals at time instant 1 and 5. $\bar{\mathcal{R}}_{k,i} = \bar{\mathcal{R}}_{k',i} = 0.5$ bps/Hz, $\bar{\mathcal{R}}_{g,k,i} = 1$ bps/Hz, and $p_s = 10$ dB. The simulated results are denoted by symbols.

In the following, we set $\mathbf{R}_T = \mathbf{I}_M$ and $L = M = N$ to unveil more system insights.

Corollary 3. When $\mathbf{R}_T = \mathbf{I}_M$ and $L = M = N$, the maximal achievable sensing rate is $\mathcal{R}_s = N \log_2 (1 + \frac{p_s}{N}) \triangleq \mathcal{R}(N)$.

By checking the first-order derivative of $\mathcal{R}(x)$ with respect to $x \geq 1$, we find that $\frac{d}{dx} \mathcal{R}(x) \geq 0$ ($x \geq 1$). Additionally, it can be found that $\lim_{N \rightarrow \infty} \mathcal{R}(N) = p_s \log_2 e$.

Remark 7. The fact of $\frac{d}{dx} \mathcal{R}(x) \geq 0$ ($x \geq 1$) suggests that the maximal achievable sensing rate, $\mathcal{R}(N)$, increases with the RadCom BS antenna number, N , monotonically.

Remark 8. The facts of $\lim_{N \rightarrow \infty} \mathcal{R}(N) = p_s \log_2 e$ and $\frac{d}{dx} \mathcal{R}(x) \geq 0$ ($x \geq 1$) indicate that the achievable sensing rate is mainly limited by the power used for radar sensing.

Turn now to the sensing rate achieved in the FDSAC system. As mentioned earlier, in FDSAC, $(1 - \alpha)$ fraction of the total bandwidth is used for radar sensing, and thus the maximal sensing rate is given by $\mathcal{R}_{s,f}^\alpha = \frac{N(1-\alpha)}{L} \max_{\text{tr}(\mathbf{S}\mathbf{S}^H) \leq p_s} \log_2 \det \left(\mathbf{I}_L + (1 - \alpha)^{-1} \mathbf{S}^H \mathbf{R}_T \mathbf{S} \right)$. We notice that $\mathcal{R}_{s,f}^\alpha$ presents a similar form as \mathcal{R}_s , which can be calculated by following the steps outlined in Appendix C.

V. RATE REGION CHARACTERIZATION

In this part, we characterize the rate region of the considered ISAC system and the baseline FDSAC system. Particularly, we use \mathcal{R}^c and \mathcal{R}^s to denote the achievable average ergodic sum communication rate and sensing rate of the system, respectively. Therefore, the communication-sensing rate region of the ISAC system can be characterized as

$$\left\{ (\mathcal{R}^c, \mathcal{R}^s) \mid 0 \leq \mathcal{R}^c \leq L^{-1} \sum_{i=1}^L \bar{\mathcal{R}}_i, 0 \leq \mathcal{R}^s \leq \mathcal{R}_s \right\}, \quad (18)$$

whereas the rate region of the FDSAC system satisfies

$$\left\{ (\mathcal{R}^c, \mathcal{R}^s) \mid 0 \leq \mathcal{R}^c \leq \mathcal{R}_{c,f}^\alpha, 0 \leq \mathcal{R}^s \leq \mathcal{R}_{s,f}^\alpha, \alpha \in [0, 1] \right\}. \quad (19)$$

VI. NUMERICAL RESULTS

In this section, numerical results will be used to demonstrate the performance of the ISAC system and also verify the accuracy of the developed analytical results. The parameters used for simulation are listed as follows: $N = 4$, $M = 4$, $L = 5$, $K = 2$, and the eigenvalues of \mathbf{R}_T are $\{5, 2, 1, 0.5\}$.

Fig. 2(a) and Fig. 2(b) present the OP and ECR of CUs versus the communication SNR p_c , respectively, where the analytical results are calculated by (8) or (10) and the asymptotic

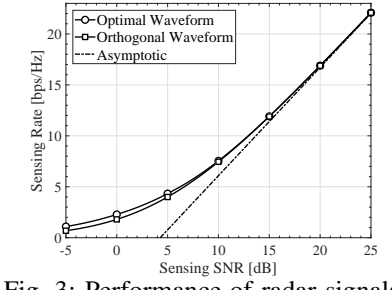


Fig. 3: Performance of radar signals.

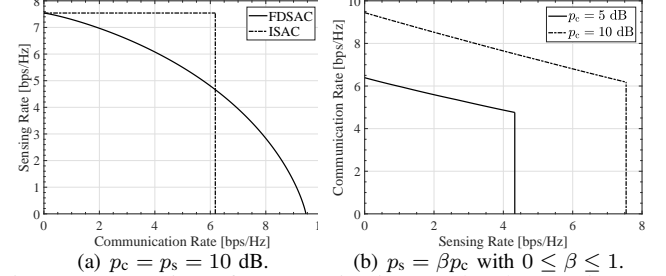


Fig. 4: Rate region of communications and radar sensing: (a) ISAC vs FDSAC; (b) Influence of radar sensing.

results are calculated by (9) or (11). We find the analytical results fit well with the simulated results and the derived asymptotic results track the numerical results accurately in the high-SNR regime. Besides, as shown in Fig. 2, the ISAC system at time instant $i = 5$ enjoys a higher ECR as well as a lower OP than that at time instant $i = 1$, which agrees with the conclusion in Remark 6. Fig. 3 plots the maximal sensing rate achieved by the optimal radar waveform versus the sensing SNR p_s , where the asymptotic results are calculated with (16). We observe the asymptotic results track the numerical results accurately in the high-SNR regime. For comparison, the sensing rate achieved by the orthogonal waveform design, i.e., $\mathbf{S}\mathbf{S}^H = \frac{p_s}{M} \mathbf{I}_M$, is also plotted. As shown, the optimal waveform outperforms the orthogonal one in terms of the sensing rate, especially in the low-SNR region. Yet, in the high-SNR regime, these two waveforms achieve virtually the same sensing rate as well as the same high-SNR slope.

Fig. 4(a) compares the rate region of the considered ISAC system (presented in (18)) and the baseline FDSAC system (presented in (19)). As shown, when achieving the same communication rate, the ISAC system yields a higher sensing rate than the FDSAC system, which highlights the superiority of the ISAC system. In this work, we assume that the communication signals can be perfectly removed by the SIC technique before the radar sensing procedure. This means that the communication signals will not influence the sensing rate. Yet, it can be observed from (5) and (6) that the radar signals can decrease the performance of communications. To illustrate this influence, Fig. 4(b) plots the rate region of the ISAC system when the sensing SNR satisfies $p_s = \beta p_c$ with various $0 \leq \beta \leq 1$. As shown, the communication rate decreases monotonically as the sensing rate increases, thus indicating a performance tradeoff between communications and sensing.

VII. CONCLUSION

Theoretical analyses characterize the communication-sensing rate region of uplink ISAC systems. It is found that

the ISAC system yields a higher sensing rate than the FDSAC system when achieving the same communication rate.

APPENDIX A PROOF OF THEOREM 1

Proof: Since the columns of \mathbf{G} are i.i.d., we can express \mathbf{G}^H as $\mathbf{G}^H = \mathbf{Q}\mathbf{R}_T^{1/2}$, where $\mathbf{Q} \in \mathbb{C}^{N \times M}$ contains NM i.i.d. complex Gaussian random variables with zero mean and unit variance. Consequently, $\mathbf{G}^H \mathbf{s}_i \sim \mathcal{CN}(\mathbf{0}, |\mathbf{s}_i^H \mathbf{R}_T \mathbf{s}_i| \mathbf{I}_N)$, which yields $\mathbb{E} \left\{ \left| \mathbf{w}_k^H \mathbf{G}^H \mathbf{s}_i \right|^2 + |n_{k,i}|^2 \right\} = |\mathbf{s}_i^H \mathbf{R}_T \mathbf{s}_i| \mathbf{w}_k^H \mathbf{w}_k + 1 = |\mathbf{s}_i^H \mathbf{R}_T \mathbf{s}_i| + 1 = \sigma^2$. Furthermore, the random variable $|\mathbf{w}_k^H \mathbf{h}_k|^2$ follows the chi-square distribution with the PDF $f_k(x) = \frac{1}{(N-2K+1)!} x^{N-2K+1} e^{-x}$ [12]. It is worth noting that \mathbf{w}_k is independent of $\mathbf{h}_{k'}$, which together with the facts of $\|\mathbf{w}_k\| = 1$ and $\mathbf{h}_{k'} \sim \mathcal{CN}(\mathbf{0}, \mathbf{I}_N)$, suggests that the random variable $|\mathbf{w}_k^H \mathbf{h}_{k'}|^2$ is exponential distributed and is independent of $|\mathbf{w}_k^H \mathbf{h}_k|^2$. Since $\|\mathbf{w}_k\| = 1$, $|\mathbf{w}_k^H \mathbf{h}_{k'}|^2$ follows the exponential distribution with the PDF $f_{k'}(x) = e^{-x}$. Based on the property of chi-square distribution, we find the random variable $|\mathbf{w}_k^H \mathbf{h}_k|^2 + |\mathbf{w}_k^H \mathbf{h}_{k'}|^2$ follows the chi-square distribution with the PDF $f_{k+k'}(x) = \frac{1}{(N-2K+2)!} x^{N-2K+2} e^{-x}$. According to (7), the OPs can be calculated as $P_{k,i} = \int_0^\infty f_{k'}(y) \int_0^{\bar{\gamma}_{k,i}(y+1/\rho)} f_k(x) dx dy$, $P_{k',i} = 1 - \int_{\bar{\gamma}_{k',i}/\rho}^\infty f_{k'}(y) \int_{\bar{\gamma}_{k,i}(y+1/\rho)}^\infty f_k(x) dx dy$, and $P_{g,k,i} = \int_0^{\bar{\gamma}_{g,k,i}/\rho} f_{k+k'}(x) dx$, respectively. Inserting the obtained PDFs into the expressions of OPs and calculating the resultant integrals, we arrive at the results in (8). When $p_c \rightarrow \infty$, using the properties of $\lim_{x \rightarrow 0} e^x = 1$, $\lim_{x \rightarrow 0} \Gamma(l+1, x) = l!$, and $\lim_{x \rightarrow 0} \frac{\Upsilon(s, x)}{x^s} \rightarrow \frac{1}{s}$ [11, eq. (8.354.1)], we can get the results in (9) after some basic manipulations. ■

APPENDIX B PROOF OF THEOREM 2

Proof: Inserting the obtained PDF expressions into the expressions of the ECRs and calculating the resultant integrals with the aid of [11, eq. (4.337.5)], we can obtain the results in (10). By continuously using $\lim_{x \rightarrow 0} e^x = 1$ and $\lim_{x \rightarrow 0} \text{Ei}(-x) = \ln x + C$ [11, eq. (8.214.2)], we can get the approximated results in (11b) and (11c) when $\rho \rightarrow \infty$. Furthermore, $\lim_{\rho \rightarrow \infty} \bar{\mathcal{R}}_{k,i} = \mathbb{E} \left\{ |\mathbf{w}_k^H \mathbf{h}_k|^2 \right\} - \mathbb{E} \left\{ |\mathbf{w}_k^H \mathbf{h}_{k'}|^2 \right\}$, which can be further rewritten as (11a). ■

APPENDIX C PROOF OF THEOREM 3

Proof: Note that \mathbf{R}_T is a positive definite matrix, and it follows the Sylvester's determinant identity that $\mathcal{I}_T = \log_2 \det \left(\mathbf{I}_L + \mathbf{S}^H \mathbf{R}_T \mathbf{S} \right) = \log_2 \det \left(\mathbf{I}_M + \mathbf{R}_T^{1/2} \mathbf{S} \mathbf{S}^H \mathbf{R}_T^{1/2} \right)$, which can be treated as the transmission rate of a virtual MIMO channel $\bar{\mathbf{y}} = \mathbf{R}_T^{1/2} \bar{\mathbf{S}} \bar{\mathbf{x}} + \bar{\mathbf{n}}$ with $\mathbb{E} \{ \bar{\mathbf{x}} \bar{\mathbf{x}}^H \} = \mathbf{I}_L$ and $\bar{\mathbf{n}} \sim \mathcal{CN}(\mathbf{0}, \mathbf{I}_M)$. Consequently, the problem defined in (14) can be optimally solved with the water-filling method. Let $\mathbf{U}_T^H \Lambda_T \mathbf{U}_T$ denote the ED of \mathbf{R}_T , where $\mathbf{U}_T^H \mathbf{U}_T = \mathbf{I}_M$ and $\Lambda_T = \text{diag} \{ \lambda_1, \dots, \lambda_M \}$ ($\lambda_1 \geq \dots \geq \lambda_M > 0$). Then, we can obtain $\mathcal{I}_T = \log_2 \det \left(\mathbf{I}_M + \Lambda_T \mathbf{U}_T \mathbf{S} \mathbf{S}^H \mathbf{U}_T^H \Lambda_T \right)$. Let

$\mathbf{V}^H \Delta \mathbf{V}$ denote the ED of $\mathbf{S} \mathbf{S}^H$, where $\mathbf{V}^H \mathbf{V} = \mathbf{I}_M$ and $\Delta = \text{diag} \{ s_1, \dots, s_M \}$ with $\sum_{m=1}^M s_m \leq p_s$. It is clear that the optimal \mathbf{V} satisfies $\mathbf{V}^* = \mathbf{U}_T$ and problem (14) can be reformulated as $\max_{\sum_{m=1}^M s_m \leq p_s} \sum_{m=1}^M \log_2 (1 + \lambda_m s_m)$. Aided with the water-filling method, we can get the optimal diagonal matrix Δ , which is denoted as $\Delta^* = \text{diag} \{ s_1^*, \dots, s_M^* \}$. Specifically, we have $s_m^* = \max \left\{ 0, \frac{1}{\nu} - \frac{1}{\lambda_i} \right\}$, where ν satisfies $\sum_{m=1}^M \max \left\{ 0, \frac{1}{\nu} - \frac{1}{\lambda_i} \right\} = p_s$ [13]. As a result, the maximal achievable sensing rate is given as $\mathcal{R}_s = \frac{N}{L} \sum_{m=1}^M \log_2 (1 + \lambda_m s_m^*)$. When the power used for sensing approaches infinity, namely $p_s \rightarrow \infty$, we have $\nu \rightarrow 0$, which yields $\sum_{m=1}^M \max \left\{ 0, \frac{1}{\nu} - \frac{1}{\lambda_i} \right\} = \frac{M}{\nu} - \sum_{m=1}^M \frac{1}{\lambda_i} = p_s$. Therefore, the high-SNR sensing rate can be written as $\mathcal{R}_s = \frac{N}{L} \sum_{m=1}^M \log_2 (\lambda_m / M) + \frac{NM}{L} \log_2 \left(p_s + \sum_{m=1}^M \frac{1}{\lambda_m} \right)$. The final result follows immediately. ■

APPENDIX D PROOF OF COROLLARY 2

Proof: According to Appendix A, we can obtain $\mathbb{E} \left\{ \left| \mathbf{w}_k^H \mathbf{G}^H \mathbf{s}_i \right|^2 \right\} = |\mathbf{s}_i^H \mathbf{R}_T \mathbf{s}_i|$. Furthermore, the optimal waveform matrix satisfies $\mathbf{S} \mathbf{S}^H = \mathbf{U}_T^H \Delta^* \mathbf{U}_T$, where $\mathbf{U}_T^H \Lambda_T \mathbf{U}_T$ denotes the ED of \mathbf{R}_T with $\mathbf{U}_T^H \mathbf{U}_T = \mathbf{I}_M$ and $\Lambda_T = \text{diag} \{ \lambda_1, \dots, \lambda_M \}$ ($\lambda_1 \geq \dots \geq \lambda_M > 0$). Consequently, we can get $\mathbf{S}^H \mathbf{R}_T \mathbf{S} = \text{diag} \{ \lambda_1 s_1^*, \dots, \lambda_M s_M^*, 0, \dots, 0 \} \in \mathbb{C}^{L \times L}$. The final result follows immediately. ■

REFERENCES

- [1] F. Liu, *et al.*, “Integrated sensing and communications: Towards dual-functional wireless networks for 6G and beyond,” *arXiv preprint arXiv:2108.07165*, 2021.
- [2] L. Zheng, *et al.*, “Radar and communication coexistence: An overview: A review of recent methods,” *IEEE Signal Process. Mag.*, vol. 36, no. 5, pp. 85–99, Sep. 2019.
- [3] F. Liu, *et al.*, “Joint radar and communication design: Applications, state-of-the-art, and the road ahead,” *IEEE Trans. Commun.*, vol. 68, no. 6, pp. 3834–3862, Jun. 2020.
- [4] J. A. Zhang, *et al.*, “An overview of signal processing techniques for joint communication and radar sensing,” *IEEE J. Sel. Topics Signal Process.*, vol. 15, no. 6, pp. 1295–1315, Nov. 2021.
- [5] P. Kumari, *et al.*, “Adaptive virtual waveform design for millimeter-wave joint communication-radar,” *IEEE Trans. Signal Process.*, vol. 68, pp. 715–730, 2020.
- [6] A. R. Chiriyath, B. Paul, G. M. Jacyna, and D. W. Bliss, “Inner bounds on performance of radar and communications co-existence,” *IEEE Trans. Signal Process.*, vol. 64, no. 2, pp. 464–474, Jan. 2016.
- [7] Z. Ding, *et al.*, “A general MIMO framework for NOMA downlink and uplink transmission based on signal alignment,” *IEEE Trans. Wireless Commun.*, vol. 15, no. 6, pp. 4438–4454, Jun. 2016.
- [8] B. Tang, J. Tang, and Y. Peng, “MIMO radar waveform design in colored noise based on information theory,” *IEEE Trans. Signal Process.*, vol. 58, no. 9, pp. 4684–4697, Sep. 2010.
- [9] B. Tang and J. Li, “Spectrally constrained MIMO radar waveform design based on mutual information,” *IEEE Trans. Signal Process.*, vol. 67, no. 3, pp. 821–834, Feb. 2019.
- [10] B. Hassibi and B. M. Hochwald, “How much training is needed in multiple-antenna wireless links?” *IEEE Trans. Inf. Theory*, vol. 49, no. 4, pp. 951–963, Apr. 2003.
- [11] I. S. Gradshteyn and I. M. Ryzhik, *Table of Integrals, Series and Products*, 7th ed., Academic, San Diego, C.A., 2007.
- [12] R. W. Heath, Jr., and A. Lozano, *Foundation MIMO Communication*, Cambridge, U.K.: Cambridge Univ. Press, 2018.
- [13] I. E. Telatar, “Capacity of multi-antenna gaussian channels,” *Europ. Trans. Telecommu.*, vol. 10, pp. 585–595, Nov./Dec. 1999.